Vol. 35, No. 1 (2013) 3-18

Tribology in Industry

www.tribology.fink.rs

RESEARCH

Shakedown Behavior in Multiple Normal Loading-Unloading of an Elastic-Plastic Spherical Stick Contact

B. Chatterjee[a], P. Sahoo[a]

[a]*Department of Mechanical Engineering, Jadavpur University, Kolkata 700032, India.*

Keywords:

Shakedown
Multiple loading-unloading
Strain hardening
Spherical contact
ANSYS

Corresponding author:

Prasanta Sahoo
Department of Mechanical Engineering, Jadavpur University, Kolkata 700032, India
E-mail: psjume@gmail.com

A B S T R A C T

The effect of strain hardening and hardening rule on shakedown behavior is studied in a multiple normal interaction process of an elastic plastic sphere against a rigid flat using finite element software ANSYS under full stick contact condition. Seven to ten repeated loading cycles are considered in the interference controlled multiple normal loading unloading depending upon the maximum interference of loading. Emphasis is placed on wide range of tangent modulus by varying the hardening parameter within the range as found for most of the practical materials with both the kinematic and isotropic hardening model, which has not yet been investigated. It is found that with small tangent modulus, the cyclic loading process gradually converges into elastic shakedown with both kinematic and isotropic strain hardening laws; similar to recently published finite element based normal loading unloading results. The effect of strain hardening laws on shakedown behavior is pronounced at higher tangent modulus. The higher dimensionless interference of loading and higher tangent modulus increase the dimensionless dissipated energy with kinematic hardening rule. The load-interference hysteretic response with varying tangent modulus using both kinematic and isotropic hardening laws is interpreted in the context of elastic and plastic shakedown.

1. INTRODUCTION

When a material is subjected to repeated normal loading-unloading, its deformation depends on the extent of the amplitude of the maximum stress with respect to the yield stress of the material. When contact stress exceeds yield stress, plastic flow of the material occurs beyond the elastic limit loading. Residual stresses, developed after complete unloading, are protective in nature as they reduce the tendency of plastic flow in the subsequent loading. Strain hardening of the material strongly affects the development of residual strain after complete unloading. The cyclic response may be perfectly elastic and reversible, stabilized and closed cycle of plastic strain or consists of repetitive accumulation of incremental unidirectional plastic strain [1-3] depending on the intensity of loading, elastic and plastic properties of the

materials and the tribological system parameters like friction, wear etc. [4]. Thus the modeling of cyclic response is quite complex. The repeated cyclic loading promotes fatigue of the deformable or softer materials. Non-conforming bodies when brought into contact without deformation, either point or line contact may occur [5]. The type of relative motion between mating surfaces produces sliding, rolling contact. The prominent contact damages encountered due to the sliding and rolling contact fatigues are galling, surface distress, spalling, pitting etc. [6]. Fretting fatigue is observed owing to the relative cyclic motion with small amplitude between two oscillating surfaces [7].

The basic step of investigating the cyclic response of rough surfaces involves the study with single asperity contact. Cattaneo [8] and then Mindlin [9] independently published the solutions for pure elastic sliding contact. Both of them assumed a central stick region surrounded by a slip annulus in the contact area. The local Coulomb's friction law governs the slip annulus region and it increases with the increase in tangential loading. The local Coulomb's friction law couples normal stress with local shear stress and the central stick region gets eliminated at the point of sliding inception. Mindlin et al. [10, 11] offered first analytical solutions for the problem of oscillating tangential loading. The derived force-displacement hysteretic loop by Mindlin et al. is concerned about the energy dissipation due to partial frictional sliding between the contacting surfaces during the loading cycles. The fretting models, which are based on the assumptions of Cattaneo-Mindilin [8,9], ignored the formation of junction growth. The authors of fretting models [12,13] also made simplified assumption that the normal contact pressure and the contact area, which resulted from the normal loading alone, remain unchanged during application of the tangential loading. Bowden and Tabor [14] described the sliding inception and static friction as a failure mechanism, which are functions of material properties. The approach of Bowden and Tabor was different from Cattaneo-Mindlin in the sense that in the former the static friction coefficient is not known a priori. Bowden and Tabor was also successful to completely decouple the maximum shear stresses at the contact interface from the normal stresses. Based on the assumptions of Bowden and Tabor, Tabor [15] further presented the concept of junction growth in metallic friction. Recently, Ovcharenko et al. [16] investigated the junction growth in elastic plastic spherical contact. The materials deform elastically following Hooke's law within elastic limit. Above elastic limit the deformation follows certain strain-hardening rule. No bodies are perfectly elastic, so during cyclic loading-unloading even within elastic limit some energy is dissipated. Tabor [17] reported the resistance to rolling of bodies of imperfectly elastic material, which can also be expressed in terms of their hysteresis loss factor. The model of rolling friction provided by Tabor was well supported by Greenwood et al. [18] in their experimental work with rubber. Tabor inferred that the theory of rolling friction does not hold good for metals. Actually hysteresis loss factor, fraction of loss of maximum strain energy stored, is not generally a material constant. Hysteresis loss is common phenomena for both stress controlled (Constant load during cyclic loading) and strain controlled (Constant interference) fatigue. The respective strain amplitude and stress amplitude during stress controlled and strain controlled cyclic loading unloading attains a stable saturation value after an initial shakedown period. This saturation provides a stable hysteresis loop.

Depending up on the nature of hysteresis loop, many authors identified the type of shakedowns in sliding contact, fretting contact, adhesive contact apart from the literatures discussed above. In the recently published research works, shakedown has been simulated in elastic plastic loading level with the use of finite element software, which can provide an accurate result of interfacial parameters during elastic plastic as well as in plastic contact. Kadin et al. [19] found plastic shake down with kinematic hardening while elastic shake down with isotropic hardening for a cyclic loading of an elastic-plastic adhesive spherical micro contact with the use of finite element software ANSYS. They also inferred that the plasticity parameter, a function of yield strength, of the material plays an important role on the shakedown behavior. Song and Komvopoulos [20] performed the finite element simulation for the adhesive contact of an elastic plastic half space with a rigid sphere using finite element software ABAQUS. They concluded that the elastic and plastic shakedown might occur even with elastic perfectly plastic

materials, depending on the plasticity parameter. They found elastic shakedown for a low plasticity parameter even under large maximum normal displacement while plastic shakedown for a high plasticity parameter under very small maximum normal displacement. Based on the fundamental of Bowden and Tabor [14], Zolotarevskiy et al. [21] simulated elastic plastic spherical contact under cyclic tangential loading in pre-sliding using ANSYS. They found that the friction-displacement loops of isotropic hardening materials exhibited elastic shakedown whereas materials with kinematic hardening shows plastic shakedown following the second cycle. The experimental results by Ovcharenko and Etsion [7] report elastic shakedown with 2.5% hardening steel spheres and plastic shakedown with elastic perfectly plastic copper spheres for elastic plastic spherical contact fretting.

The type of hardening model and the intensity of strain hardening greatly affect the interfacial parameters of a spherical contact during repeated normal loading unloading. It is pertinent to mention here that the changes in contact geometry are more pronounced in purely normal loading rather than during rolling or sliding contact. Most of the theoretical studies on normal loading unloading of a spherical contact assumed frictionless contact with bilinear isotropic hardening or with the elastic perfectly plastic material. Kral et al. [22] inferred that the effect of strain hardening on the contact parameters during loading unloading in the elastic plastic region is severe in comparison with the less significant effect of elastic properties of the material. They simulated the repeated normal indentation of an elastic plastic half space by a rigid sphere assuming a hardening power law, where the strain-hardening exponent was varied up to 0.5, to study the effect of strain hardening. They also observed that the hardening materials reached a shakedown in respect to accumulation of plastic strain after three to four repeated normal loading unloading under perfect slip contact condition with isotropic hardening. Chatterjee and Sahoo [23] offered a model for loading unloading of a deformable sphere against a rigid flat to study the effect of strain hardening under perfect slip contact condition assuming a hardening parameter which enabled them to study the effect of tangent modulus as high as 33% of modulus of elasticity. They found that the higher strain hardening caters less resistance to full recovery of the original shape. They noted that the load interference path for the second loading coincides with the first unloading path for the elastic perfectly plastic material as well as the materials with high tangent modulus under perfect slip contact condition with bilinear isotropic hardening. Thus the multiple loading unloading of a deformable sphere against a rigid flat under perfect slip contact condition is reversible. Then Chatterjee and Sahoo [24] extended their study to investigate the effect of strain hardening in elastic plastic loading of a deformable sphere against a rigid flat under full stick contact condition. They also considered both the isotropic and kinematic hardening rules. The only finite element based multiple loading unloading of a deformable sphere against a rigid flat under full stick contact condition with isotropic and kinematic hardening is available so far in the literature is the simulation generated by Zait et al. [25]. They considered only 2% bilinear hardening and their load displacement loop exhibited vanishing dissipated energy, which resulted in elastic shakedown for both isotropic and kinematic hardening. The same result of hysteresis loop with both the hardening model provides a ground to study the effect of strain hardening with varying tangent modulus using the model of Zait et al. [25]. Hence the main goal of the present study is to investigate the effect of strain hardening on the hysteretic behavior of repeated normal loading unloading of a deformable sphere against a rigid flat under full stick contact condition considering both the isotropic and kinematic hardening models.

2. MULTIPLE NORMAL LOADING-UNLOADING MODEL

The deformable sphere with a rigid flat is shown in Fig. 1. The dashed and solid lines in the figure show the position of sphere and the rigid flat before and after the loading respectively. The interference (ω), the contact radius (a) of the deformable sphere of radius R, correspond to an external load (P) applied to the contact are presented in the Fig. 1. The expressions of critical interference, ω_c, which initiates the yield inception at first loading and the corresponding critical load Pc under full stick condition are

given by Brizmer et al. [26], which are used to normalized the contact parameters.

$$\omega_c = (C_v \frac{\pi(1-\nu^2)}{2}(\frac{Y}{E}))^2 R(6.82\nu - 7.83(\nu^2 + 0.0586)) \quad (1)$$

$$P_c = \frac{\pi^3 Y}{6} C_v^3 (R(1-\nu^2)(\frac{Y}{E}))^2 (8.88\nu - 10.13(\nu^2 + 0.089)) \quad (2)$$

Where $C_v = 1.234 + 1.256\nu$. The parameters Y, E, and ν are the virgin yield stress, the Young modulus, and Poisson's ratio of the sphere material, respectively and R is the radius of the sphere. The sphere size used for this analysis is R = 1 μm. The material properties used here are Young's Modulus (E) = 70 GPa, Poisson's Ratio (ν) = 0.3 and Yield stress (Y) = 100 MPa.

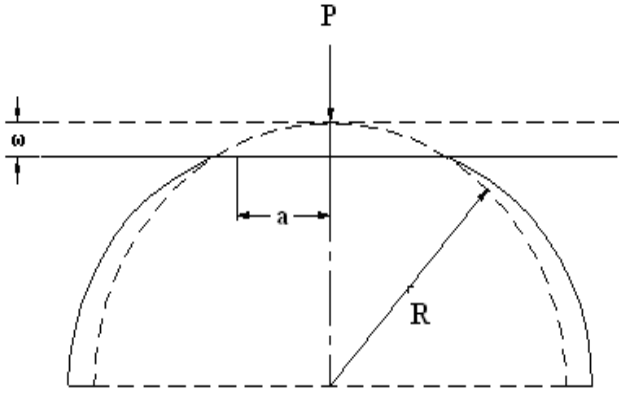

Fig. 1. A deformable sphere pressed by a rigid flat.

Multiple normal loading unloading cycle consists two stages. First the rigid flat gradually loads the deformable sphere to a dimensionless interference ω_{max}/ω_c, which results a dimensionless loading P_{max}/P_c. The plastic zone evolves within contact region inside the sphere. During the second stage of unloading, the interference (ω) is gradually reduced. At the completion of the unloading, under zero contact load and contact area, the sphere has locked-in residual stresses and strain.

The residual stresses and strains, which remain locked in the sphere results in a deformed unloaded sphere and the amount depends on the hardening ratio (E_t/E) [27]. Therefore the original un-deformed spherical geometry is not fully recovered. The normal loading unloading cycle, to the same ω_{max}/ω_c, is performed seven to ten times considering both isotropic and kinematic hardening models to study the effect of strain hardening as well as hardening rule on the hysteretic behavior under full stick contact condition.

3. THE FINITE ELEMENT MODEL

The commercial finite element software ANSYS 11.0 is used to get the response of the repeated normal loading unloading of the elastic plastic sphere against a rigid flat. The sphere is modeled as quarter of a circle due to the advantage of simulation of axisymmetric problems. A line models the rigid flat. Six node triangular axisymmetric elements (plane183) are used in the present model. Plane183 has plasticity, hyperelasticity, creep, stress stiffening, large deflection, and large strain capabilities along with the capability for simulating deformations of nearly incompressible elastoplastic materials, and fully incompressible hyperelastic materials [28]. The mesh consists of maximum 18653 six node triangular axisymmetric elements (plane183) comprising 37731 nodes. The resulting ANSYS mesh is presented in Fig. 2. The mesh density at the bottom of the sphere is coarsest one and is made gradually finer towards the sphere summit. The finest mesh density near the contact region simultaneously allows the sphere's curvature to be captured and accurately simulated during deformation with a reduction in computation time. Window 2 of Fig. 2 presents the enlarged view of the finest mesh density at sphere summit. The sphere surface is modeled with the contact elements CONTA172 and the rigid flat is modeled by a single, non-flexible two-node target surface element TARGE169. The nodes lying on the axis of symmetry of the hemisphere are restricted to move only in the radial direction. Likewise the nodes in the bottom of the hemisphere are fixed in both the axial and radial direction. For full stick contact condition, infinite friction condition is adopted. Both the bilinear kinematic hardening (BKIN) and bilinear isotropic hardening (BISO) options are considered to study the effect of hardening rule on the hysteretic loop during the repeated normal loading unloading. The rate independent plasticity algorithm incorporates the von Mises criterion. The mesh density is gradually doubled until the contact force and contact area differed by less than 1% between the iterations. In addition to mesh convergence, the model also compares well with the Hertz elastic solution at interferences below the critical interference for perfect slip contact condition. This work uses Lagrangian multiplier method. The tolerance of current work is set to 1% of the element width.

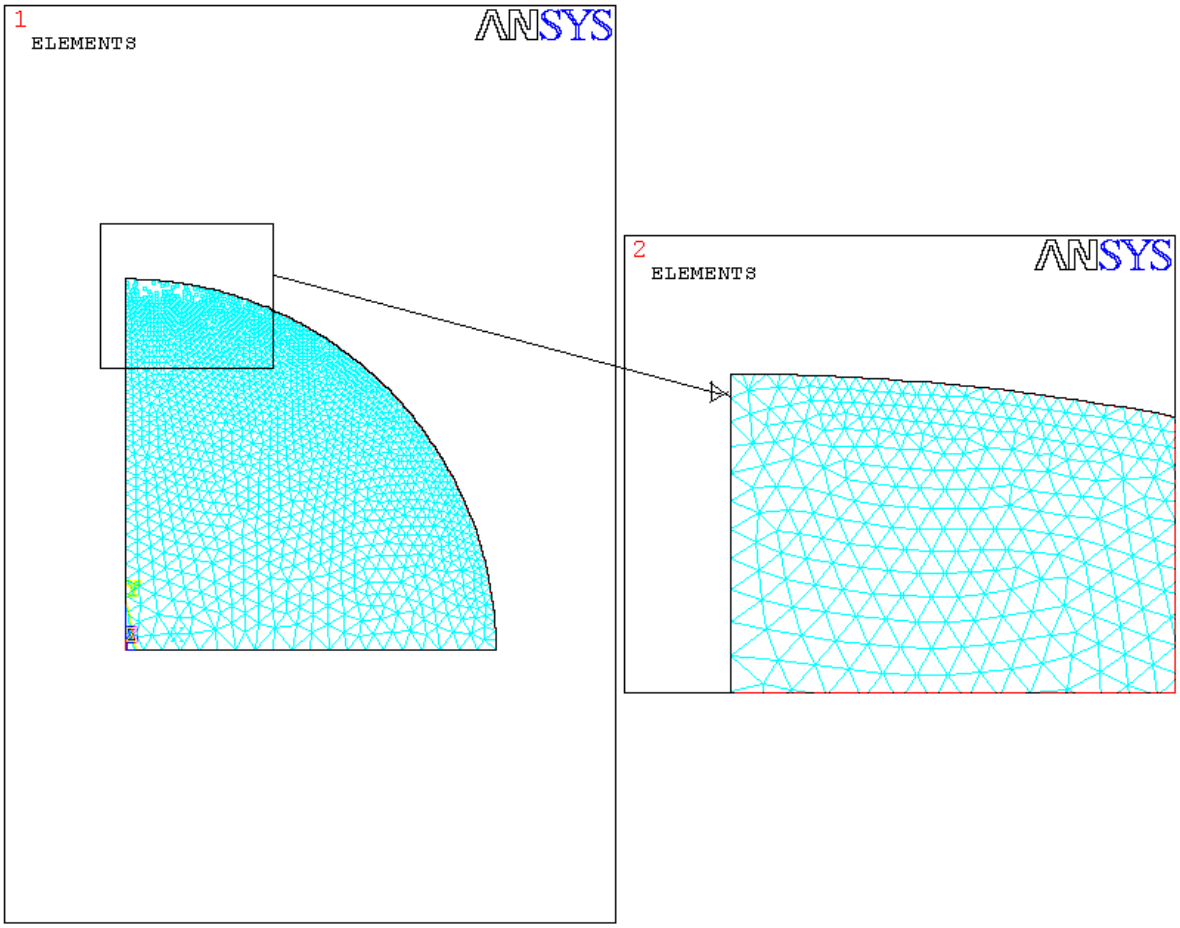

Fig. 2. Finite element mesh of a sphere generated by ANSYS.

Engineering stress-strain curves are used within elastic limit. The dimension of the specimen changes substantially in the region of plastic deformation. The increment of strain in conjunction with true stress can be termed as strain hardening. Strain hardening causes an increase in strength and hardness of the metal. Strain hardening is expressed in terms of tangent modulus (E_t), which is the slope of the stress-strain curve. Below the proportional limit, the tangent modulus is the same as the Young's modulus (E). Above the proportional limit, the tangent modulus varies with the strain. The tangent modulus is useful in describing the behaviour of materials that have been stressed beyond the elastic region. In elastic perfectly plastic cases, the tangent modulus becomes zero. Very few materials exhibit elastic perfectly plastic behaviour, generally all the materials follow the multi-linear behaviour with some tangent modulus. This multi-linear behaviour can be modelled as bilinear behaviour for analysis purpose in elastic-plastic cases. In this analysis a bilinear material property, as shown in Fig. 3, is provided for the deformable sphere.

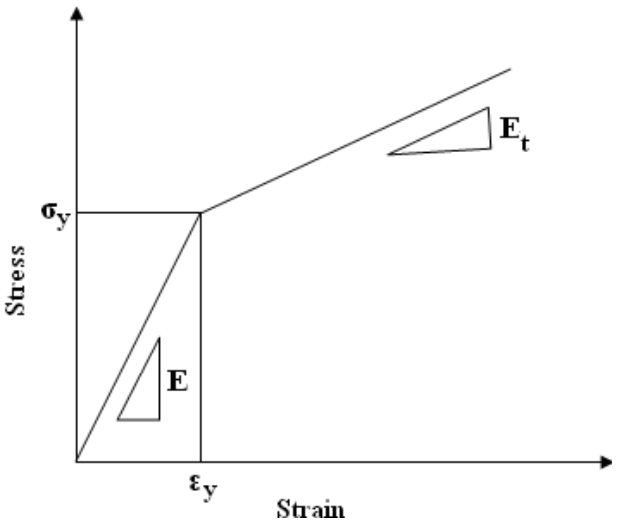

Fig. 3. Stress-strain diagram for a material with bilinear properties.

4. RESULTS AND DISCUSSIONS

It is already stated that the aim of the present study is to investigate the influence of strain hardening and the hardening model on the hysteretic loop. Shankar and Mayuram [29] mentioned that the tangent modulus for the most practical materials is less than 0.05 E, whereas Kadin et al. [27] found the tangent modulus for most practical materials below 0.02 E. However both the authors used tangent modulus up to 0.1E for analytical purpose. On the other hand, Ovcharenko et al. [30] used stainless steel specimen with tangent modulus of 0.26 E (Fig. 6(b)) in their in-situ investigation). It is also available in literature that structural steel, aluminum alloys have significant amount of strain hardening. Zait et al. [25] found elastic shakedown with two percent kinematic hardening. Thus first multiple normal loading-unloading is simulated with elastic perfectly plastic material and the elastic plastic sphere with 2.5 and 5 percent bilinear hardening using both isotropic and kinematic hardening.

Figure 4 presents dimensionless normal contact load as a function of dimensionless normal interference during ten multiple loading-unloading cycles for maximum dimensionless interference, ω_{max}=100.

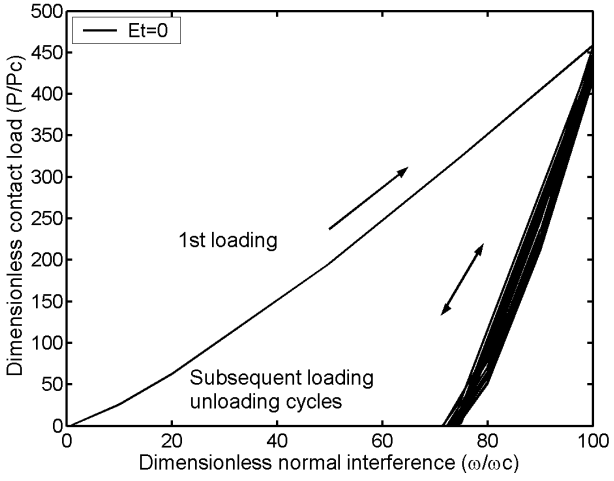

Fig. 4. Dimensionless normal contact load vs. dimensionless interference hysteretic loop for maximum loading, ω^*_{max}=100.

The sphere material is considered as elastic perfectly plastic. Interference controlled multiple loading unloading is adopted. It is found that the response of the elastic perfectly plastic materials during multiple loading-unloading with both the isotropic and kinematic hardening is identical. The area bounded by dimensionless interference and dimensionless contact load after first unloading under full stick contact condition, the quantity of dissipated energy, clearly indicates elastic shakedown.

Figure 5 shows the load interference hysteretic loop during ten repeated loading unloading. The maximum dimensionless interference for loading is ω^*_{max}=100, with tangent modulus, E_t= 0.025E using kinematic hardening.

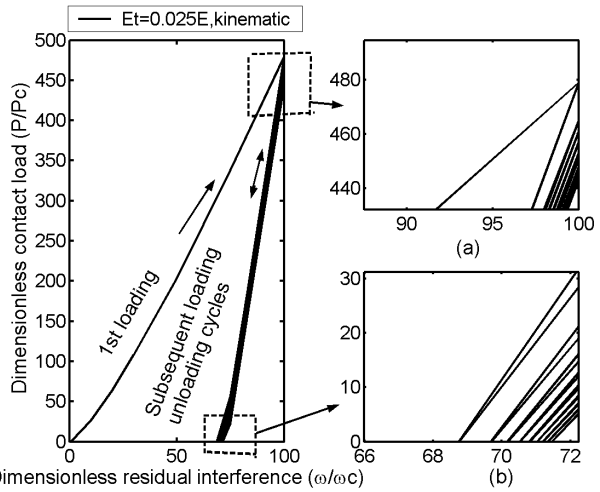

Fig. 5. Dimensionless normal contact load vs. dimensionless interference hysteretic loop for maximum loading, ω^*_{max}=100 with kinematic hardening.

The elastic shakedown with vanishing dissipated energy even with kinematic hardening is prominent from the figure. Zait et al. [25] furnished the results (Fig. 4) with maximum dimensionless interference of 60 using kinematic hardening. They have shown that with small tangent modulus the materials result in elastic shakedown even under the influence of kinematic hardening. The present simulated results are in good agreement with the findings of Zait et al. [25]. The right top figure (a) here, enlarged view of contact load after each loading cycle, shows the decrease of contact load during ten repeated loading cycles, using 2.5% bilinear kinematic hardening, under full stick contact condition. The bottom right figure (b), detailed view of residual interferences after each unloading cycles, presents the increase of residual interferences during ten repeated loading unloading cycles with 2.5% bilinear kinematic hardening under full stick contact condition.

Figure 6 represents the load interference hysteretic loop during ten repeated loading-unloading cycles under full stick contact condition. The simulation used 2.5% bilinear isotropic hardening for the maximum dimensionless loading up to ω^*_{max}=100. Here also the elastic plastic deformable sphere yields in elastic shakedown. The right top figure (a) indicates the decrease of dimensionless contact load during ten repeated loading cycles. The bottom right figure (b) presents the increase of residual interferences after each unloading cycles during ten loading unloading cycles. Comparing the results of Figs. 5 and 6, it is observed that the decrease of contact load after tenth loading cycles and increase of residual interference after ten loading unloading cycles with both hardening rule is almost identical with vanishing dissipated energy.

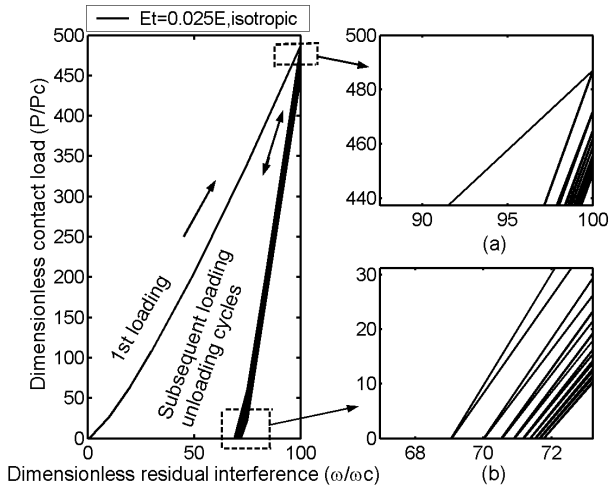

Fig. 6. Dimensionless normal contact load vs. dimensionless interference hysteretic loop for maximum loading, ω^*_{max}=100 with isotropic hardening.

Figure 7(a) presents the hysteretic loop of the dimensionless normal contact load with respect to dimensionless interference during ten repeated loading unloading cycles under full stick contact condition with 5% bilinear isotropic hardening. The maximum dimensionless interference of loading is ω^*_{max}=100. The figure reveals the elastic shakedown with vanishing dissipated energy as expected for isotropic hardening. Figure 7(b) is the plot of the hysteretic loop under full stick contact condition with 5% bilinear kinematic hardening. The maximum dimensionless interference of loading during ten repeated loading unloading cycles is ω^*_{max}=100.

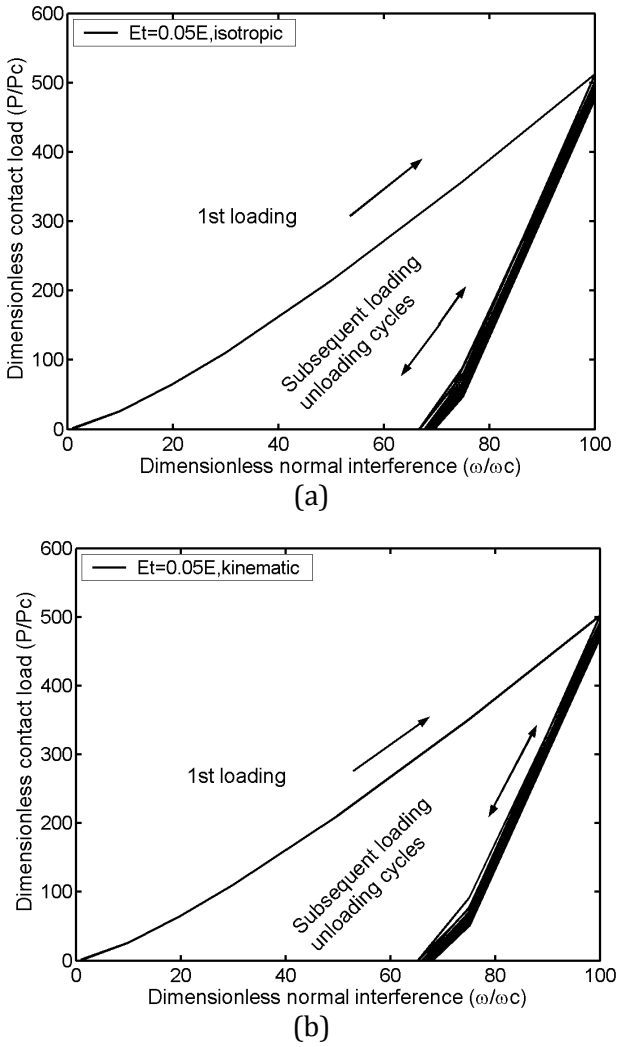

Fig. 7. Dimensionless normal contact load vs. dimensionless interference hysteretic loop for maximum loading, ω^*_{max}=100 with (a) isotropic hardening (b) kinematic hardening.

Here also the figure indicates the elastic shakedown even with kinematic hardening. Zait et al. [25] also observed that under full stick contact condition the deformable sphere resulted in elastic shakedown with 2% bilinear kinematic hardening for normal repeated loading. They attributed the similar shakedown behavior with both hardening models to the small variation of the von Mises stress.

As can be seen from Figs. 4 to 7, the deformable sphere shows elastic shakedown with both the hardening models for repeated normal loading unloading under full stick contact condition. The results show excellent agreement with the results of Zait et al. [25]. Zait et al. did not consider the effect of high tangent modulus on the multiple normal loading-unloading of a deformable sphere against a rigid flat. Kral et al.

[22] used strain-hardening exponent to study the effect of strain hardening on the deformation of an elastic plastic half space against a rigid sphere during repeated loading unloading. They reported that the hardening materials (strain hardening exponent up to 0.5) reached to a shakedown in light of accumulation of plastic strain after three to four repeated normal loading unloading cycles under perfect slip contact condition with isotropic hardening. The tangent modulus of stainless steel, structural steel, aluminum alloys etc. are 15% or above the modulus of elasticity of the respective materials. Thus in the next part of present analysis, the tangent modulus (E_t) is varied according to a hardening parameter (H). The hardening parameter is defined as:

$$H = \frac{E_t}{E - E_t}.$$

The present analysis considered four different values of H, covering wide range of tangent modulus to depict the effect of strain hardening in single asperity multiple loading unloading contact analysis with other material properties being constant. The values of H used in this analysis are within range $0 \le H \le 0.5$ as most of the practical materials falls in this range [31]. The value of H equals to zero indicates elastic perfectly plastic material behavior, which is an idealized material behavior. The hardening parameters used for this analysis and their corresponding E_t values are shown in Table 1.

Table 1. Different H and E_t values used for the study of strain hardening effect.

H	E_t in %E	E_t (GPa)
0	0.0	0.0
0.1	9.0	6.3
0.3	23.0	16.1
0.5	33.0	23.1

Figure 8(a) is the plot of hysteretic loop of dimensionless normal contact load versus dimensionless interference under full stick contact condition for the elastic perfectly plastic material. The maximum dimensionless interference of loading in this interference controlled repeated normal loading unloading is ω^*_{max}=50. The figure indicates vanishing dissipated energy, which resulted in elastic shakedown. Figure 8(b) shows the resulted hysteretic loop of the dimensionless normal contact load versus dimensionless interference under full stick contact condition for the elastic perfectly plastic material. Here the maximum dimensionless interference of loading in the interference controlled repeated loading unloading is 200. It is clear from Figs. 8(a) and 8(b) that the increase of the loading interference exhibits no effect on the shakedown behaviour as hysteretic loop in both the figure indicate vanishing dissipated energy.

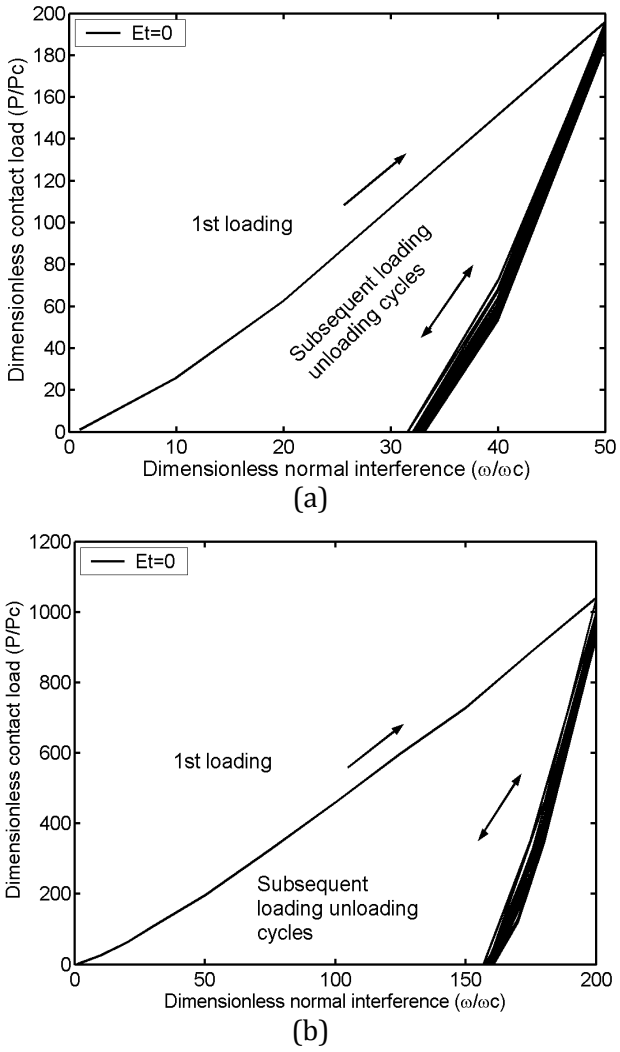

Fig. 8. Dimensionless normal contact load vs. dimensionless interference hysteretic loop for maximum loading, (a) ω^*_{max}=50 (b) ω^*_{max}=200.

Figure 9 presents the dimensionless contact load as a function of dimensionless interference during ten normal loading unloading cycles under full stick contact condition for the sphere material with hardening parameter, H=0.1. The hysteretic loop considering bilinear isotropic

hardening with tangent modulus (E_t) equals to 9% of elastic modulus clearly converged into elastic shakedown. The right top figure (a) shows the slight decrease of dimensionless contact load in interference controlled repeated normal loading with maximum interference of loading equals to ω^*_{max}=50 while bottom right figure (b) presents the increase of residual interferences after each unloading cycles.

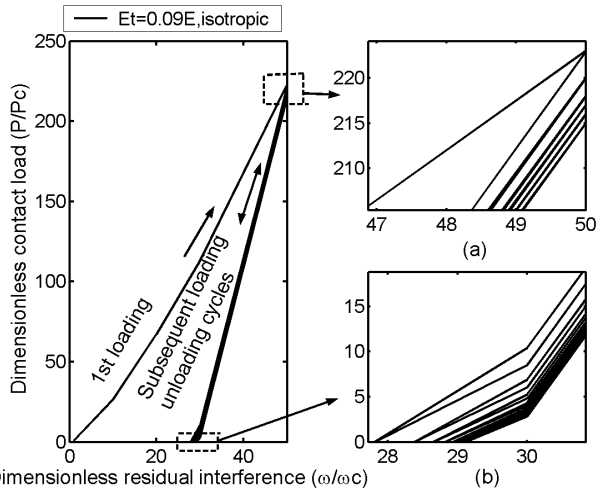

Fig. 9. Dimensionless normal contact load vs. dimensionless interference hysteretic loop for maximum loading, ω^*_{max}=50.

Hysteretic loop of repeated normal loading unloading for the deformable sphere with hardening parameter, H=0.1 considering kinematic hardening under full stick contact condition is plotted in Fig. 10(a). The figure reveals more dissipated energy with kinematic hardening compared to the dissipated energy with isotropic hardening.

The top Fig. of 10 (b) shows the evolution of contact load after each loading cycles during ten repeated loading unloading cycles with tangent modulus, E_t=0.09E. The maximum dimensionless interference of loading is 50.

The bottom Fig. of 10(b) exhibits the residual interference after each unloading cycles. Comparing the results with two different hardening models, it is found that the contact load at the end of maximum dimensionless interference with kinematic hardening is greater than the contact load with isotropic hardening. Similar behaviour is also observed elsewhere [24]. On the other hand, the residual interference with kinematic hardening is lesser than that of with isotropic hardening.

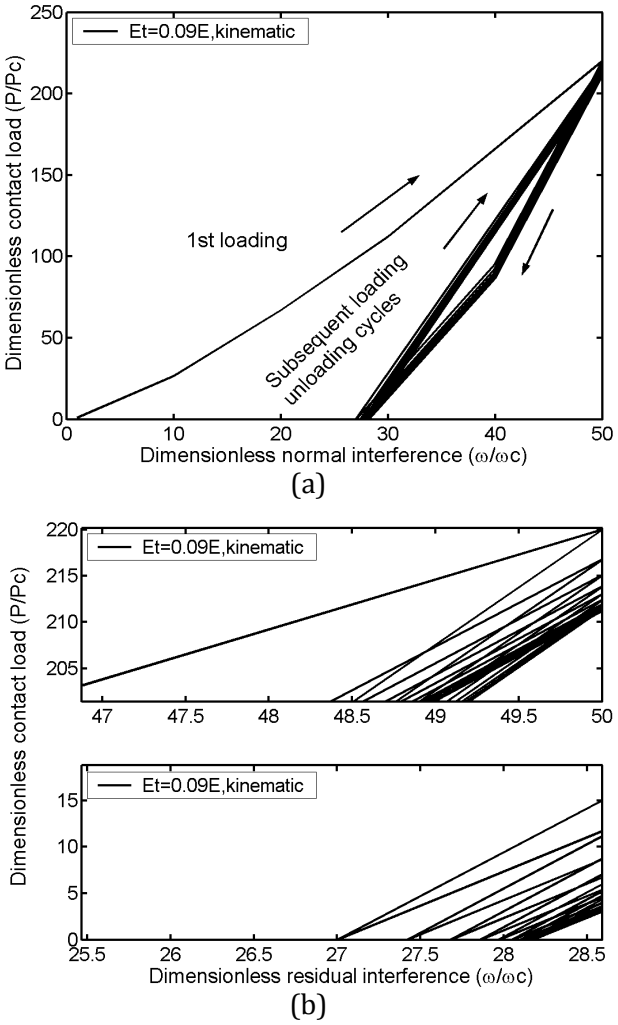

Fig. 10. (a) Dimensionless normal contact load vs. dimensionless interference hysteretic loop for maximum loading, ω^*_{max}=50 with kinematic hardening (b) Decrease of contact load and increase of residual interferences during ten loading unloading cycles.

The dimensionless normal contact load as a function of the dimensionless normal interference is presented in Fig. 11(a). The hysteretic loop, area bounded by unloaded cycle and loading cycle after first loading, with maximum dimensionless interference of 200 shows that the value of the bounded area subsequently decreasing in nature. Thus the repeated ten loading unloading cycles under full stick contact condition with isotropic hardening converges into elastic shakedown even with large interference. The area of the hysteretic loop between the unloading curve and the subsequent loading curve of dimensionless contact load and dimensionless interference under full stick contact condition presents the amount of dissipated energy. The Fig. 11(b) indicates a constant dissipation of energy after first unloading cycle. Thus it is evident that the material with high tangent modulus and kinematic hardening resulted

in plastic shakedown. It can also be seen from the figure that the area of the hysteretic loop increases with the increase in maximum dimensionless interference of loading in the interference controlled repeated loading unloading.

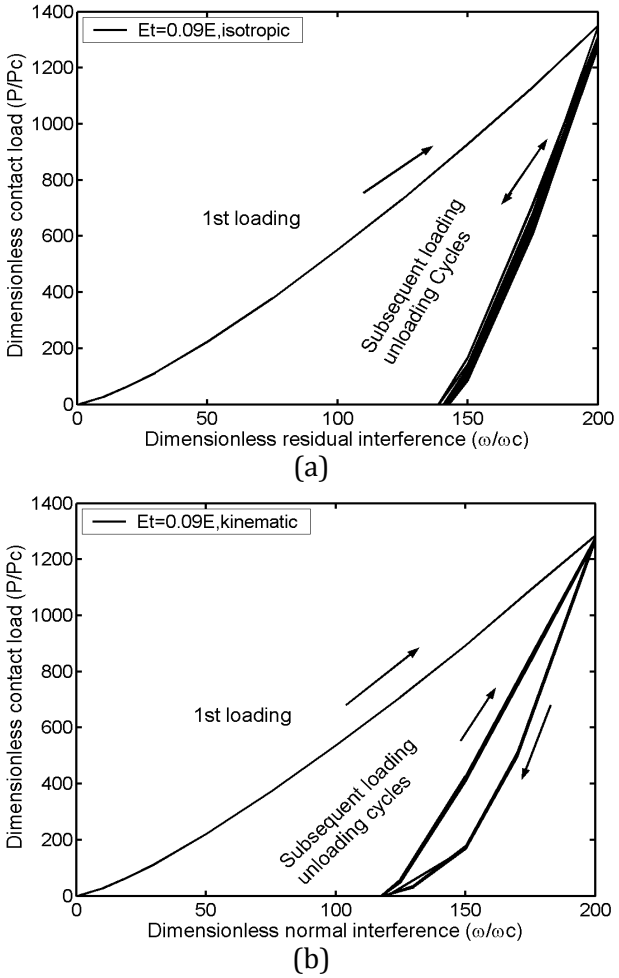

Fig. 11. Dimensionless normal contact load vs. dimensionless interference hysteretic loop for maximum loading,ω^*_{max}=200 with (a) isotropic hardening (b) kinematic hardening.

Figure 12(a) to 12(c) presents the dimensionless elastic plastic load displacement results during repeated normal loading unloading process in terms of P* vs. ω^* under full stick contact condition. The simulations have done with the hardening parameter of the sphere material, H=0.3 (tangent modulus, E_t=0.23E) using isotropic hardening. The maximum dimensionless interferences of loading for Figs. 12(a), 12(b) and 12(c) are 50, 100 and 200 respectively. We have considered ten repeated loading unloading cycles for the maximum loading interference of 50 and 100 while seven loading unloading cycles for the loading interference of 200. The hysteretic loop, the area between the unloading curve and loading curve on and from first unloading cycle of load displacement figure, shows no remarkable dissipation of energy. The vanishing nature of dissipated energy resulted in elastic shakedown. These findings are in good agreement with Kadin et al. [19] where the authors concluded that the elastic shakedown is associated with isotropic hardening.

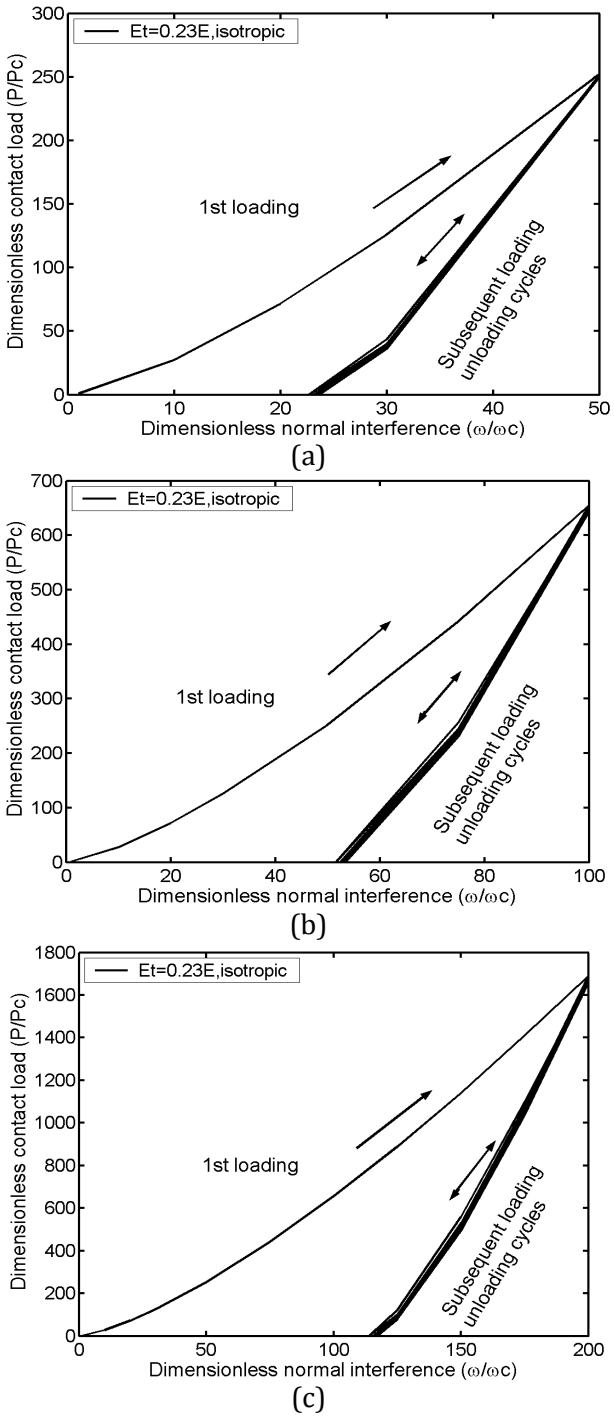

Fig. 12. Dimensionless normal contact load vs. dimensionless interference hysteretic loop for maximum loading, (a) ω^*_{max}=50, (b) ω^*_{max}=100, (c) ω^*_{max}=200.

The dimensionless normal contact loads as a function of normal dimensionless interferences under full stick contact condition are plotted in Fig. 13 (a) to 13(c). The hardening parameter chosen for these simulations is, H=0.3 (tangent modulus, E_t=0.23E) using kinematic hardening. It reveals from the figures that the unloading curves and the loading curves are identical on and from second cycle exhibiting constant dimensionless energy dissipation (the area of the hysteretic loop) during each repeated cycle. Here also we have used ten repeated cycles for the maximum interference loading of 50 and 100, whereas seven repeated cycles for the maximum interference loading of 200. The constant dimensionless energy dissipation indicates plastic shakedown as would be expected for kinematic hardening. It is also observed from Fig. 13(a) to 13(c) that the dissipated energy increases with the increase in maximum interference of loading.

Figure 14, the details of Fig. 13(c), presents the evolution of dimensionless contact load and dimensionless residual interferences during repeated loading unloading. It is found from the figure (a) that the dimensionless contact load is almost identical from second loading cycles and figure (b) indicates that the increase in dimensionless residual interference is also negligible after repeated unloading cycles. Comparison of two hardening model also reveals that the dimensionless contact load for the same dimensionless interference is larger with isotropic hardening than that of with kinematic hardening. However the effect of hardening model is more pronounced during unloading, the materials with kinematic hardening offer less resistance to recovery of original shape compared to the materials associated with isotropic hardening.

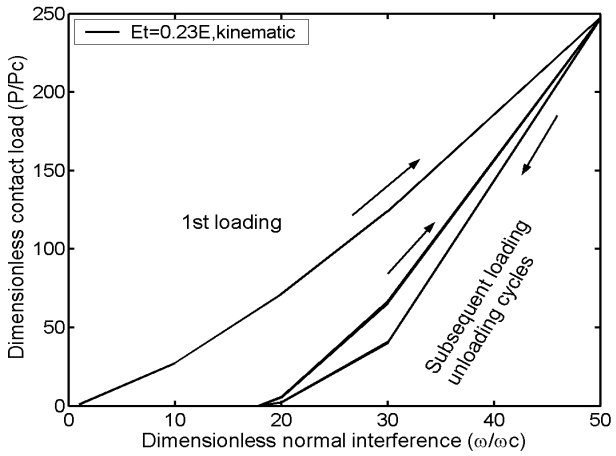

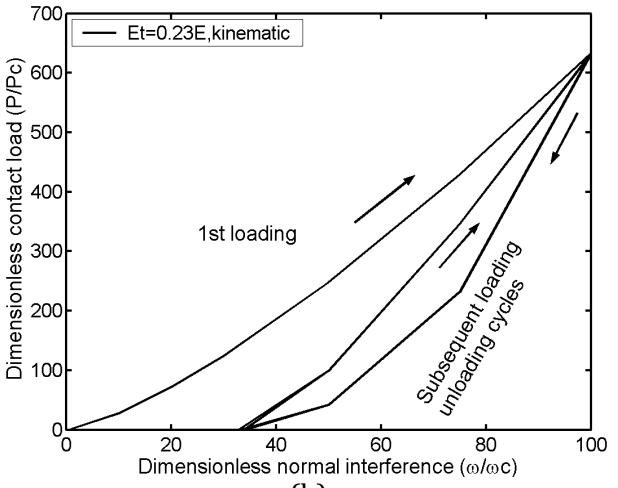

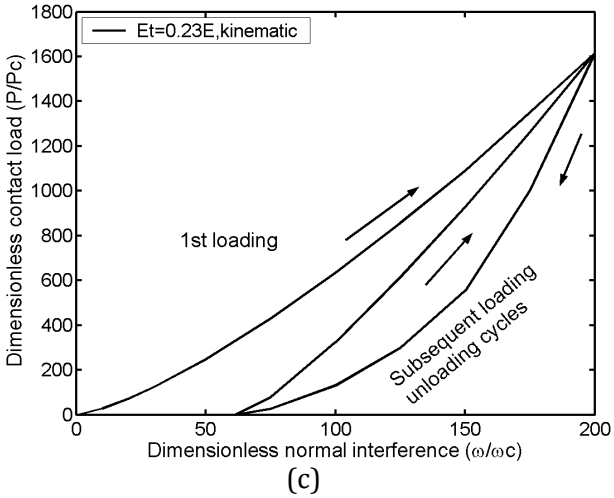

Fig. 13. Dimensionless normal contact load vs. dimensionless interference hysteretic loop for maximum loading, (a) ω^*_{max}=50, (b) ω^*_{max}=100, (c) ω^*_{max}=200.

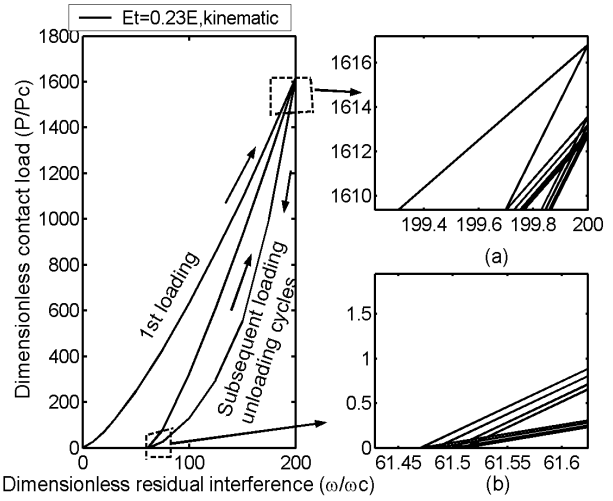

Fig. 14. Evolution of contact load and residual interferences during repeated loading unloading of plastic shakedown process.

Figure 15(a) to 15(c) presented the effect of maximum dimensionless interference of loading

in interference controlled repeated loading unloading on the evolution of dimensionless normal contact load versus dimensionless normal interference for repeated loading unloading cycles. Ten repeated loading unloading cycles are considered when the maximum dimensionless interferences are 50 and 100. Seven repeated loading unloading cycles are simulated for maximum dimensionless interference loading of 200. The load displacement loop of the sphere material with hardening parameter, H=0.5 (tangent modulus, E_t=0.33E) using isotropic hardening exhibiting convergence to an elastic shakedown irrespective of the extent of maximum interference of loading. Thus the shakedown behavior in case of normal repeated loading unloading depends predominantly on the hardening rule and tangent modulus of the deformable sphere rather than the extent of loading in the interference controlled repeated loading unloading.

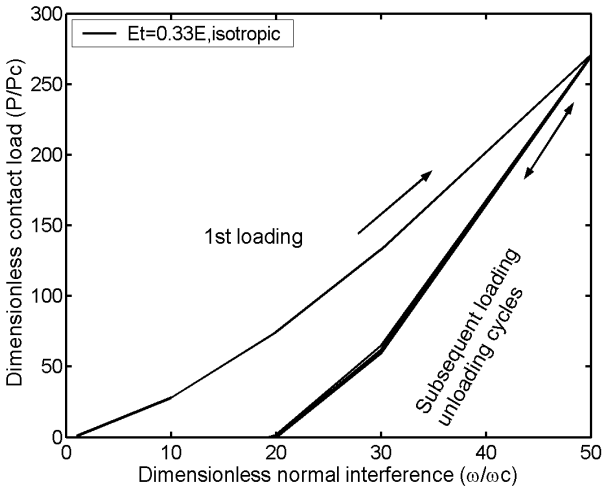

(a)

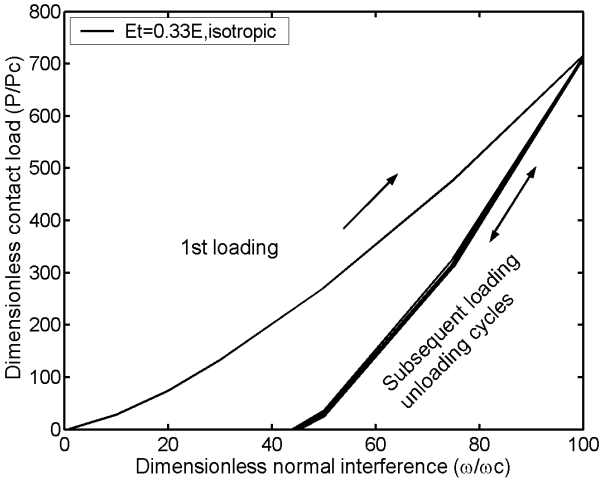

(b)

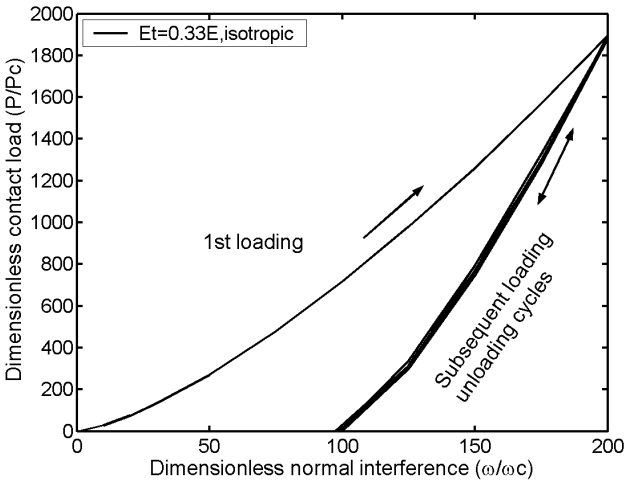

(c)

Fig. 15. Dimensionless normal contact load vs. dimensionless interference hysteretic loop for maximum loading, (a) ω^*_{max}=50, (b) ω^*_{max}=100, (c) ω^*_{max}=200.

The dimensionless normal contact load versus dimensionless normal interference in repeated loading unloading for a deformable sphere with a rigid flat under full stick contact condition using kinematic hardening are shown in Fig. 16(a) to 16(c). The maximum dimensionless interferences of loading for the sphere material with tangent modulus, E_t=0.33E (Hardening parameter, H=0.5) are 50,100 and 200 respectively. Ten repeated loading unloading cycles are used for the maximum dimensionless loading interferences of 50 and 100 although seven such repeated cycles are used foe the maximum loading interference of 200. It reveals from the figures that the load-displacement hysteretic loops, irrespective of the maximum dimensionless interferences of loading, exhibited constant dissipated energy indicating plastic shakedown.

From the several simulations it was found that in order to enable a common basis for the comparison of the dimensionless dissipated energy, the energy transferred to the deformable sphere during first loading is to be kept constant. Thus the dissipated energy is normalized with the product Pω of elastic perfectly plastic materials. The dissipated energy is calculated by numerically integrating the area enclosed within the hysteretic load-displacement loop. The effects of strain hardening (E_t/E) on the constant dissipated energy at plastic shakedown are shown for maximum dimensionless loading interference of 50, 100 and 200 in Figs. 17(a), 17(b) and 17(c) respectively. As can be observed from the figures, the constant dissipated energy during plastic shakedown increases with the increase in

the tangent modulus of the deformable sphere. Comparing the results for the different maximum dimensionless interference of loading, it is evident that the constant dissipation energy during plastic shakedown is increasing with the increase in maximum dimensionless interference of loading for a specific tangent modulus of the sphere material. Zolotarevskiy et al. [21] found that the constant dissipated energy during plastic shakedown increases with the increase in dimensionless normal load while simulating under tangential loading in pre-sliding under full stick contact condition. Our results for repeated normal loading unloading under full stick contact condition correlate well with Zolotarevskiy et al. [21] in regards to the effect of normal load on constant dissipated energy during plastic shakedown.

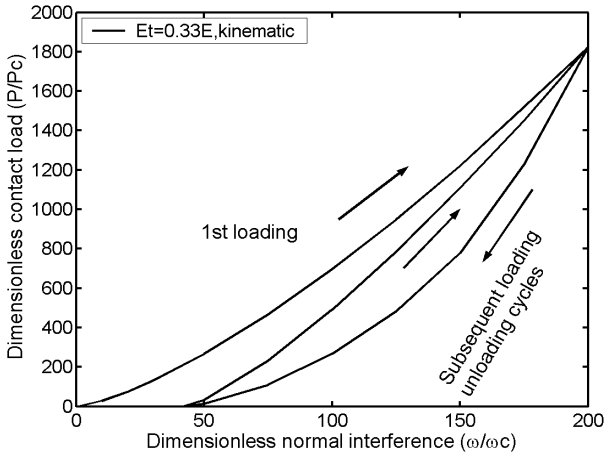

(c)

Fig. 16. Dimensionless normal contact load vs. dimensionless interference hysteretic loop for maximum loading, (a) ω^*_{max}=50, (b) ω^*_{max}=100, (c) ω^*_{max}=200.

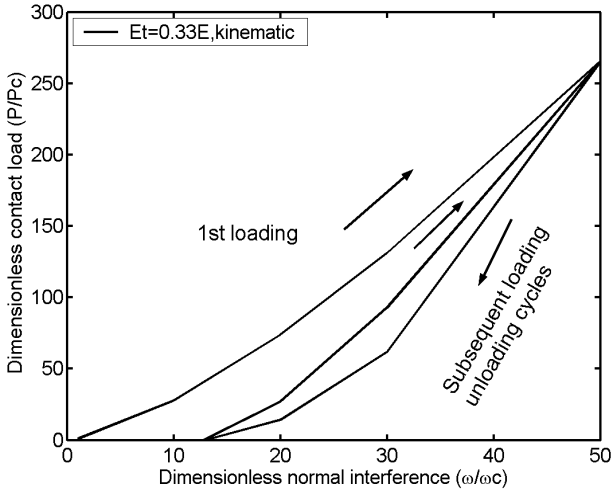

(a)

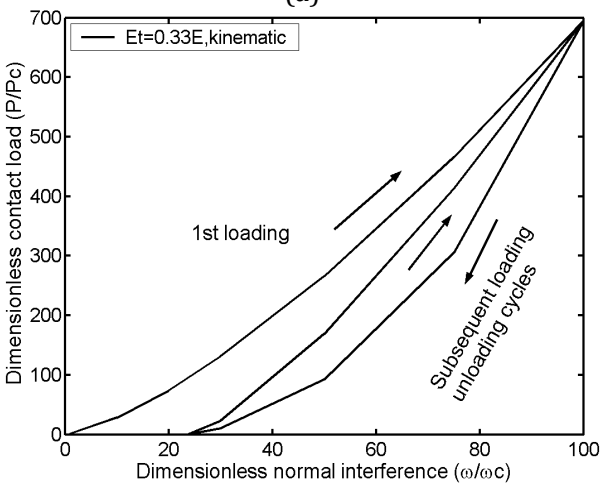

(b)

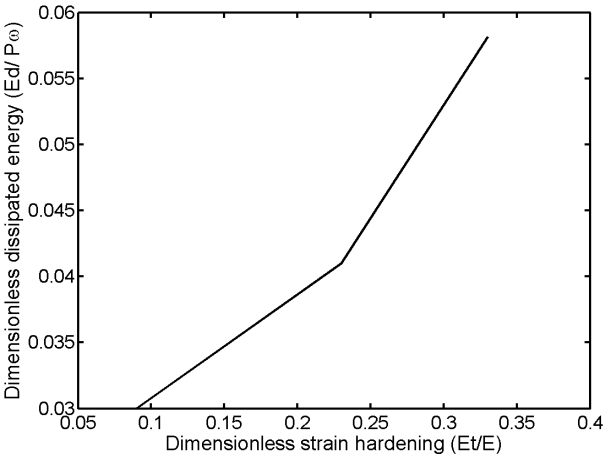

(a)

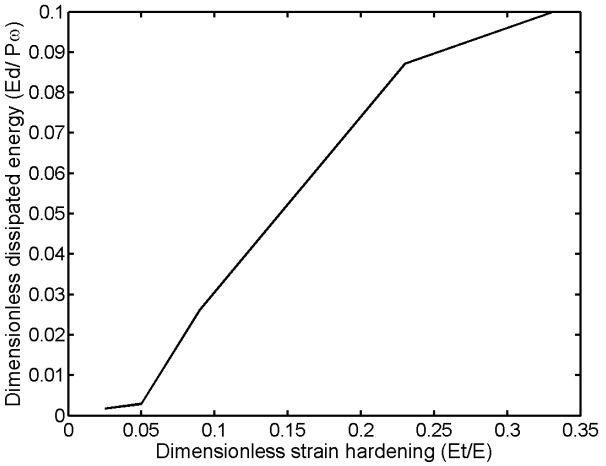

(b)

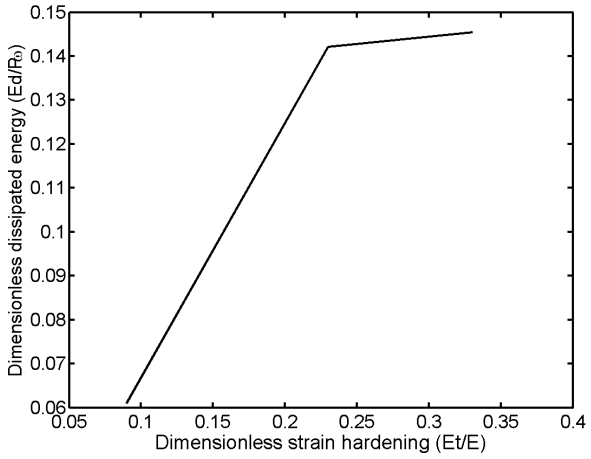

(c)

Fig. 17. Dimensionless dissipated energy vs. E_t/E at (a) ω^*_{max}=50, (b) ω^*_{max}=100, (c) ω^*_{max}=200.

The present study considers the shakedown behavior in full stick contact condition for varying tangent modulus. However, there are other material parameters like Poisson's ratio, work hardening, ratio of elastic modulus to yield strength etc. that need to be considered [32]. Also other contact conditions like pure slip and stick-slip need to be considered in future studies. The present study assumes non-adhesive contact situation but a realistic contact analysis should include the presence of adhesion [33]. Future work will consider such contact situations.

5. CONCLUSIONS

The elastic plastic spherical contact subjected to repeated normal loading unloading under full stick contact condition with varying tangent modulus was analyzed using commercial finite element software ANSYS. Both the isotropic and kinematic hardening rules were studied. The elastic shakedown for isotropic hardening and plastic shakedown for kinematic hardening was predicted for most of the published results of sliding, fretting and rolling contact repetitive loading. Recently published finite element based multiple normal loading unloading of a deformable sphere against a rigid flat converged into elastic shakedown with both 2% bilinear isotropic and kinematic hardening. The present results within 5% hardening were found qualitatively similar elastic shakedown with both isotropic and kinematic hardening as inferred in recently published finite element based results. The sphere material with high tangent modulus (from 9% to 33% of elastic modulus), as observed in stainless steel, structural steel and different aluminum alloys, exhibited constant dissipated energy (plastic shakedown) following the second loading cycles with kinematic hardening and converges into elastic shakedown with isotropic hardening. It was also found that elastic plastic spherical contact with isotropic hardening produced more dimensionless contact load than the elastic plastic spherical contact with kinematic hardening particularly for high tangent modulus. The residual interferences with kinematic hardening after complete unloading is less compared to the residual interferences simulated with isotropic hardening, which, in turn, offers less resistance to full recovery of the original shape with kinematic hardening. The results from present simulation also revealed that the higher dimensionless interference of loading and higher tangent modulus increase the dimensionless dissipated energy.

NOMENCLATURE

a	Contact area radius
E	Modulus of elasticity of the sphere
Y	Yield Strength of the sphere material
A	Real contact area
R	Radius of the sphere
P	Contact load
ω	Interference
ν	Poisson's ratio of sphere
p	Mean contact pressure
E_t	Tangent modulus of the sphere
P*	Dimensionless contact load, P/P_c in stick contact
A*	Dimensionless contact area, A/A_c in stick contact
ω*	Dimensionless interference,ω/ω_c in stick contact

Subscripts

c	critical values
res	Residual values following unloading
max	Maximum values during loading-unloading process

Superscripts

*	Dimensionless

REFERENCES

[1] C.P. Jones, W.R. Tyfor, J.H. Beynon, A. Kapoor: *The effect of strain hardening on shakedown limits of a pearlitic rail steel*, J. Rail Rapid Transit, Vol. 211, pp. 131-140, 1997.

[2] A. Kapoor, K.L. Johnson: *Plastic ratcheting as a mechanism of metallic wear*, Proc. R. Soc. Lond., Vol. A445, pp. 367-381, 1994.

[3] S. Fouvry, Ph. Kapsa, L. Vincent: *An elastic-plastic shakedown analysis of fretting wear*, Wear, Vol. 247, pp. 41-54, 2001.

[4] U. Olofsson, R. Lewis: *Handbook of Railway Vehicle Dynamics*, Taylor & Francis Group, LLC, 2006.

[5] K.L. Johnson: *Contact Mechanics*, Cambridge University Press, Cambridge, MA, 1985.

[6] S. Suresh: *Fatigue of Materials*, Cambridge University Press, Cambridge, MA, 1998.

[7] A. Ovcharenko, I. Etsion: *Junction growth and energy dissipation at the very early stage of elastic-plastic spherical contact fretting*, ASME J. Tribol., Vol. 131, pp. 1-8, 2009.

[8] C. Cattaneo: *sul contatto di due corpi elastici: distribuzione locale degli sforzi, Rendiconti dell*, Accademia Nazionale dei lincei 27, Ser. 6, pp. 342-348,434-436,474-478, 1938.

[9] R.D. Mindlin: *Compliance of elastic bodies in contact*, ASME J. Appl. Mech., Vol. 16, pp. 259-268, 1949.

[10] R.D. Mindlin, W.P. Mason, J.F. Osmer, H. Deresiewicz: *Effects of an oscillating tangential force on the contact surfaces of elastic spheres*, in: *Proceedings of the 1st US National Congress of Applied Mechanics-1951*, ASME, New York, pp. 203-208, 1952.

[11] R.D. Mindlin, H. Deresiewicz: *Elastic spheres in contact under varying oblique forces*, ASME J. Appl. Mech., Vol. 20, pp. 327-344, 1953.

[12] M. Odfalk, O. Vingsbo: *An elastic-plastic model for fretting contact*, Wear, Vol. 157, pp. 435-444, 1992.

[13] M. Eriten, A.A. Polycarpou, L.A. Bergman: *Physics-based modeling for partial slip behavior of spherical contacts*, Int. J. Solids Struct., Vol. 47, pp. 2554-2567, 2010.

[14] F.P. Bowden, D. Tabor: *The friction and lubrication of solids*, Clarendon Press, Oxford, 1954.

[15] D. Tabor: *Junction growth in metallic friction: the role of combined stresses and surface contamination*, Proc. R. Soc. Lond., Vol. A251. pp. 378-393, 1959.

[16] A. Ovcharenko, G. Halperin, I. Etsion: *In situ and real-time optical investigation of junction growth in spherical elastic-plastic contact*, Wear, Vol. 264, pp. 1043-1050, 2008.

[17] D. Tabor: *The mechanism of rolling friction: the elastic range*, Proc. R. Soc. Lond., Vol. A229, pp. 198-220, 1955.

[18] J.A. Greenwood, J. Minshall, D. Tabor: *Hysteresis losses in rolling and sliding friction*, Proc. R. Soc. Lond., Vol. A259, pp. 480-507, 1961.

[19] Y. Kadin, Y. Kligerman, I. Etsion: *Loading-unloading of an elastic-plastic adhesive spherical micro contact*, J. Colloid Interface Sci., Vol. 321, pp. 242-250, 2008.

[20] Z. Song, K. Komvopoulos: *Adhesion-induced instabilities in elastic and elastic-plastic contacts during single and repetitive normal loading*, J Mech. Phys. Solids, Vol. 59, pp. 884-897, 2011.

[21] V. Zolotarevskiy, Y. Kligerman, I. Etsion: *Elastic-plastic spherical contact under cyclic tangential loading in pre-sliding*, Wear, Vol. 270, pp. 888-894, 2011.

[22] E.R. Kral, K. Komvopoulous, D.B. Bogy: *Elastic-plastic finite element analysis of repeated indentation of a half-space by a rigid sphere*, ASME J. Appl. Mech., Vol. 60, pp. 829-841, 1993.

[23] B. Chatterjee, P. Sahoo: *Effect of strain hardening on unloading of a deformable sphere loaded against a rigid flat- A finite element study*, Int. J. Engg. Tech., Vol. 2, No. 4, pp. 225-233, 2010.

[24] B. Chatterjee, P. Sahoo: *Effect of strain hardening on elastic-plastic contact of a deformable sphere against a rigid flat under full contact condition*, Advances in Tribology, Vol. 2012, pp. 1-8, 2012.

[25] Y. Zait, V. Zolotarevskiy, Y. Kligerman, I. Etsion: *Multiple normal loading cycles of a spherical contact under stick contact condition*, ASME J. Tribology, Vol. 132, pp. 1-7, 2010.

[26] V. Brizmer, Y. Kligerman, I. Etsion: *The effect of contact conditions and material properties on the elasticity terminus of a spherical contact*, Int. J. Solids Struct., Vol. 43, pp. 5736-5749, 2006.

[27] Y. Kadin, Y. Kligerman, I. Etsion: *Multiple loading-unloading of an elastic-plastic spherical contact*, Int. J. Solids Struct., Vol. 43, pp. 7119-7127, 2007.

[28] ANSYS theory manual, Release 11.0, ANSYS Inc, Camonburg, USA, 2007.

[29] S. Shankar, M.M. Mayuram: *Effect of strain hardening in elastic-plastic transition behavior in a hemisphere in contact with a rigid flat*, Int. J. Solids Struct., Vol. 45, pp. 3009-3020, 2008.

[30] A. Ovcharenko, G. Halperin, G. Verberne, I. Etsion: *In situ investigation of the contact area in elastic-plastic spherical contact during loading-unloading*, Tribol. Lett., Vol. 25, pp. 153-160, 2007.

[31] F. Wang, L.M. Keer: *Numerical simulation for three-dimensional elastic-plastic contact with hardening behavior*, ASME J. Tribology, Vol. 127, No. 3, pp. 494-502, 2005.

[32] B. Chatterjee, P. Sahoo: *Elastic-plastic contact of a deformable sphere against a rigid flat at varying material properties under full stick contact condition*, Tribology in Industry, Vol. 33, No. 4, pp. 164-172, 2011.

[33] A. Mitra, P. Sahoo, K. Saha: *A multi-asperity model of contact between a smooth sphere and a rough flat surface in presence of adhesion,* Tribology in Industry, Vol. 33, No. 1, pp. 3-10, 2011.